

Reduction of the K^* meson abundance in heavy ion collisions

Sungtae Cho¹ and Su Houn Lee²

¹*Division of Science Education, Kangwon National University, Chuncheon 200-701, Korea*

²*Institute of Physics and Applied Physics, Yonsei University, Seoul 120-749, Korea*

We study the K^* meson reduction in heavy ion collisions by focusing on the hadronic effects on the K^* meson abundance. We evaluate the absorption cross sections of the K^* and K meson by light mesons in the hadronic matter, and further investigate the variation in the meson abundances for both particles during the hadronic stage of heavy ion collisions. We show how the interplay between the interaction of the K^* meson and kaon with light mesons in the hadronic medium determines the final yield difference of the statistical hadronization model to the experimental measurements. For the central Au+Au collision at $\sqrt{s_{NN}} = 200$ GeV, we find that the K^*/K yield ratio at chemical freeze-out decreases by 36% during the expansion of the hadronic matter, resulting in the final ratio comparable to STAR measurements of 0.23 ± 0.05 .

PACS numbers: 14.40.Df, 25.75.Dw, 13.75.Lb

I. INTRODUCTION

Relativistic heavy ion collision experiments have enabled the production of a system of quantum chromodynamic (QCD) matter at extreme conditions under controlled conditions [1–5]. Due to the huge energies available in heavy ion collisions, it is expected that a possible phase transition predicted by Lattice QCD [6] between a hadronic matter and a system of deconfined quarks and gluons takes place, and the quark-gluon plasma (QGP) at very high temperature is produced at the initial stage of the collision. As a result, large numbers of hadronic particles are produced during the quark-hadron phase transition at later stages of heavy ion collisions.

These hadronic particles are believed to emerge at the transition point with the information of the matter. The statistical hadronization model has been quite success in explaining the measured production yields of hadrons with two parameters characterizing the chemical freeze-out point in heavy ion collisions; the phase transition temperature and the baryon chemical potential [7–10].

All particles produced at the freeze-out, however, are subject to further interactions with other hadrons in the hadronic matter, leading to possible deviations in the final yield of some hadrons from the statistical model prediction. In addition to the effects from hadronic interactions, the lifetime of hadrons as well as the lifetime of the hadronic matter itself plays an important role in changing the abundance of hadrons from the yield at the chemical freeze-out.

The abundance of hadrons stable against strong decays is expected to be changed mostly by hadronic interactions while that of resonances will be affected by both their interactions with other hadrons and their strong decays when the lifetime of resonances is comparable to, or smaller than the lifespan of the hadronic stage in heavy ion collisions. Daughter particles of resonances are subject to re-scatter as well in the hadronic medium, making the reconstruction of the resonances from an invariant mass analysis difficult.

Studying the effects from the hadronic interactions on the abundance of resonances has been suggested as one way of confirming the scenario about a time delay between the chemical and thermal freeze-out [11, 12], since a sudden hadronization in heavy ion collisions would leave no time for resonances to decay in the hadronic medium. In particular, the K^* meson has attracted lots of attentions as its short lifetime 4 fm/c is less than the presumed lifespan of the hadronic stage.

The effects of hadronic interactions on the yield of the K^* meson have been measured in heavy ion collisions using K^*/K yield ratios. Since the K meson is the ground state of the K^* meson, having the same valence quarks with a different mass and relative orientation of its quark spins, the K^*/K yield ratio is considered to be independent of the freeze-out conditions when hadronic interactions are neglected. It has been shown that K^*/K yield ratios decrease with the increasing size of the system at the same energy [13, 14]. Compared to p+p collisions, K^*/K yield ratios in Cu+Cu and Au+Au collisions are smaller, naively implying that K^* and K mesons participate in re-scattering processes during the expansion of hadronic matter, and that the hadronic effects become larger as the size of the hadronic matter increases.

The average transverse momentum of the K^* meson measured in heavy ion collisions [13, 14], which is higher than that of the K meson in p+p collisions, also supports the re-scattering scenario about K^* mesons. K^* mesons with low transverse momenta escape the hadronic stage later than K mesons with higher transverse momenta, and thus suffer more re-scattering in the hadronic medium. As a result the measurement of the K^*/K yield ratio 0.23 ± 0.05 [13] in Au+Au collision at $\sqrt{s_{NN}} = 200$ GeV is smaller than the statistical model expectation 0.33 ± 0.01 at that collision [10]. However, as we will see, the measurement of the K^*/K yield ratio inconsistent with the statistical model prediction not only confirms the hadronic effects on the yield of the K^* meson but also provides information on the change in the properties of the hadronic matter at freeze-out.

With these measurements of the K^*/K yield ratio in

mind, we study here the hadronic effects on the K^* meson by evaluating its absorption cross sections with pions, ρ , K , and K^* mesons, and furthermore investigate variations in the K^* meson abundance during the hadronic stage of heavy ion collisions by solving a time evolution equation for the K^* meson. After the K^* meson is produced at the chemical freeze-out, it interacts mostly with light hadrons during the expansion of the hadronic matter. As a result, K^* mesons can be absorbed by the co-moving light mesons, or additionally produced from scattering between them. Thus, evaluating the K^* meson cross sections by light hadrons is necessary in estimating the hadronic effects on the K^* meson abundance in heavy ion collisions. By comparing our results with the experimental observation in heavy ion collisions, we understand the discrepancy of the K^* meson yield between the statistical model and the experimental measurements.

As has been stated, the scattering of the K^* meson daughter particles such as kaons in the hadronic medium also contains useful information in understanding the hadronic effects on K^* mesons. Therefore, we also take into account interactions of the kaon with light mesons during the hadronic stage of heavy ion collisions.

To this end, we introduce effective Lagrangians for interactions between light mesons. The effective Lagrangian methods have been used to calculate the scattering cross sections between J/ψ and hadrons in order to estimate the amount of J/ψ suppression in the hadronic matter [15–18]. Recently, similar approaches have been applied to investigate the hadronic effects on the abundance of exotic mesons such as $D_{sJ}(2317)$ [19] and $X(3872)$ mesons [20, 21].

This paper is organized as follows. In Sec. II, we first consider interactions of both the K^* meson and kaon with light mesons. Then we evaluate the absorption cross sections of both mesons in the hadronic medium using effective Lagrangians. In Sec. III we investigate the time evolution of the K^* meson abundance by solving the kinetic equation. In Sec. IV, we argue the important roles of the abundance ratio of K^* mesons to kaons in heavy ion collisions. Sec. IV is devoted to conclusions.

We have used throughout the work the isospin averaged mass for all hadrons, based on experimentally measured masses [22], e.g., $m_K = 495.645$ MeV.

II. HADRONIC EFFECTS ON K^* AND K MESONS

We first investigate hadronic interactions of a K^* meson during the hadronic stage of heavy ion collisions. The

K^* meson produced at the chemical freeze-out can be absorbed or even produced through interactions between mostly light mesons during the expansion of the hadronic matter. We consider here K^* meson interacting with the pions, ρ , K , and K^* ; $K^*\pi \rightarrow \rho K$, $K^*\rho \rightarrow \pi K$, $K^*\bar{K} \rightarrow \rho\pi$, $K^*\bar{K}^* \rightarrow \pi\pi$, and $K^*\bar{K}^* \rightarrow \rho\rho$. The diagrams representing each process are shown in Fig. 1. We introduce the following Lagrangians to describe the interaction between the K^* meson and other two mesons;

$$\begin{aligned}\mathcal{L}_{\pi K K^*} &= ig_{\pi K^* K} K^{*\mu} \vec{\tau} \cdot (\bar{K} \partial_\mu \vec{\pi} - \partial_\mu \bar{K} \vec{\pi}) + \text{H.c.}, \\ \mathcal{L}_{\rho K K} &= ig_{\rho K K} (K \vec{\tau} \partial_\mu \bar{K} - \partial_\mu K \vec{\tau} \bar{K}) \cdot \vec{\rho}^\mu, \\ \mathcal{L}_{\rho K^* K^*} &= ig_{\rho K^* K^*} [(\partial_\mu K^{*\nu} \vec{\tau} \bar{K}_\nu^* - K^{*\nu} \vec{\tau} \partial_\mu \bar{K}_\nu^*) \cdot \vec{\rho}^\mu \\ &\quad + (K^{*\nu} \vec{\tau} \cdot \partial_\mu \vec{\rho}_\nu - \partial_\mu K^{*\nu} \vec{\tau} \cdot \vec{\rho}_\nu) \bar{K}^{*\mu} \\ &\quad + K^{*\mu} (\vec{\tau} \cdot \vec{\rho}^\nu \partial_\mu \bar{K}_\nu^* - \vec{\tau} \cdot \partial_\mu \vec{\rho}^\nu \bar{K}_\nu^*)],\end{aligned}\quad (1)$$

obtained from free pseudoscalar and vector meson Lagrangians by introducing the minimal substitution. In Eq. (1), $K \equiv (K^0, K^+)$ and $K^* \equiv (K^{*0}, K^{*+})$ denote strangeness pseudoscalar and vector meson doublets, respectively, and $\vec{\pi}$ and $\vec{\rho}$ denote the pion and ρ meson isospin triplets, respectively, with Pauli matrices $\vec{\tau}$. $g_{\pi K^* K}$, $g_{\rho K K}$, and $g_{\rho K^* K^*}$ are strong coupling constants, for which we use the empirical values, $g_{\pi K^* K} = 3.25$, $g_{\rho K K} = 3.05$ [23]. We apply the SU(3) flavor symmetry to obtain $g_{\rho K^* K^*} = g_{\pi K^* K} = 3.25$.

Using the above interaction Lagrangians we evaluate the amplitudes for all processes shown in Fig. 1. The amplitudes of the K^* meson absorption by pions, ρ , K , and K^* mesons, without isospin factors and before summing and averaging over external spins, are represented by

$$\begin{aligned}\mathcal{M}_{K^*\pi \rightarrow \rho K} &\equiv \mathcal{M}_{K^*}^{(a)} + \mathcal{M}_{K^*}^{(b)} \\ \mathcal{M}_{K^*\rho \rightarrow \pi K} &\equiv \mathcal{M}_{K^*}^{(c)} + \mathcal{M}_{K^*}^{(d)} \\ \mathcal{M}_{K^*\bar{K} \rightarrow \rho\pi} &\equiv \mathcal{M}_{K^*}^{(e)} + \mathcal{M}_{K^*}^{(f)} \\ \mathcal{M}_{K^*\bar{K}^* \rightarrow \pi\pi} &\equiv \mathcal{M}_{K^*}^{(g)} + \mathcal{M}_{K^*}^{(h)} \\ \mathcal{M}_{K^*\bar{K}^* \rightarrow \rho\rho} &\equiv \mathcal{M}_{K^*}^{(i)} + \mathcal{M}_{K^*}^{(j)}\end{aligned}\quad (2)$$

where the amplitudes for the first $K^*\pi \rightarrow \rho K$ and the second process $K^*\rho \rightarrow \pi K$ are

$$\begin{aligned}\mathcal{M}_{K^*}^{(a)} &= g_{\pi K^* K} g_{\rho K^* K^*} \epsilon_1^\alpha \epsilon_3^{*\beta} \frac{1}{t - m_{K^*}^2 + im_{K^*} \Gamma_{K^*}} \left(-g^{\mu\nu} + \frac{(p_1 - p_3)^\mu (p_1 - p_3)^\nu}{m_{K^*}^2} \right) (p_2 + p_4)_\mu \\ &\quad \times \left((2p_1 - p_3)_\beta g_{\alpha\nu} - (p_1 + p_3)_\nu g_{\alpha\beta} - (p_1 - 2p_3)_\alpha g_{\beta\nu} \right),\end{aligned}$$

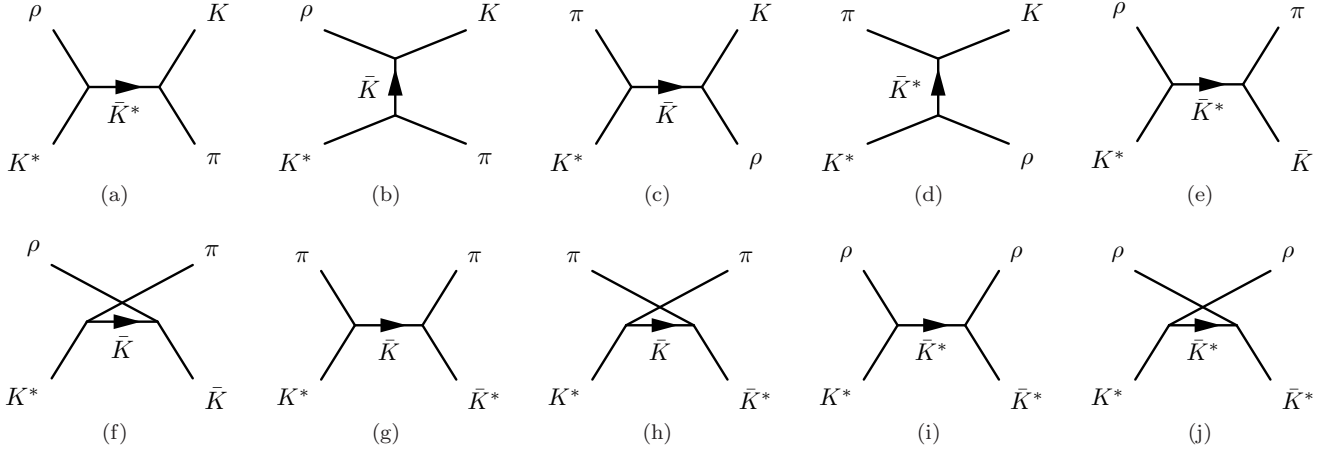


FIG. 1: Born diagrams for the K^* meson absorption by pions, ρ , K , and K^* mesons. $K^*\pi \rightarrow \rho K$, (a) and (b); $K^*\rho \rightarrow \pi K$, (c) and (d); $K^*\bar{K} \rightarrow \rho\pi$, (e) and (f); $K^*\bar{K}^* \rightarrow \pi\pi$, (g) and (h); $K^*\bar{K}^* \rightarrow \rho\rho$, (i) and (j).

$$\mathcal{M}_{K^*}^{(b)} = -g_{\pi K^* K} g_{\rho K K} \epsilon_1^\mu \epsilon_3^{*\nu} \frac{1}{s - m_K^2} (p_1 + 2p_2)_\mu (p_3 + 2p_4)_\nu, \quad (3)$$

and

$$\begin{aligned} \mathcal{M}_{K^*}^{(c)} &= -g_{\pi K^* K} g_{\rho K K} \epsilon_1^\mu \epsilon_2^\nu \frac{1}{t - m_K^2} (p_1 - 2p_3)_\mu (2p_4 - p_2)_\nu, \\ \mathcal{M}_{K^*}^{(d)} &= -g_{\pi K^* K} g_{\rho K^* K^*} \epsilon_1^\alpha \epsilon_2^\beta \frac{1}{s - m_{K^*}^2 + im_{K^*} \Gamma_{K^*}} \left(-g^{\mu\nu} + \frac{(p_1 + p_2)^\mu (p_1 + p_2)^\nu}{m_{K^*}^2} \right) (p_3 - p_4)_\mu \\ &\quad \times \left((2p_1 + p_2)_\beta g_{\alpha\nu} - (p_1 - p_2)_\nu g_{\alpha\beta} - (p_1 + 2p_2)_\alpha g_{\beta\nu} \right), \end{aligned} \quad (4)$$

respectively. Similarly, amplitudes for processes $K^*\bar{K} \rightarrow \rho\pi$ and $K^*\bar{K}^* \rightarrow \pi\pi$ are

$$\begin{aligned} \mathcal{M}_{K^*}^{(e)} &= g_{\pi K^* K} g_{\rho K^* K^*} \epsilon_1^\alpha \epsilon_3^{*\beta} \frac{1}{t - m_{K^*}^2 + im_{K^*} \Gamma_{K^*}} \left(-g^{\mu\nu} + \frac{(p_1 - p_3)^\mu (p_1 - p_3)^\nu}{m_{K^*}^2} \right) (p_2 + p_4)_\mu \\ &\quad \times \left((2p_3 - p_1)_\alpha g_{\beta\nu} - (p_1 + p_3)_\nu g_{\alpha\beta} + (2p_1 - p_3)_\beta g_{\alpha\nu} \right), \\ \mathcal{M}_{K^*}^{(f)} &= g_{\pi K^* K} g_{\rho K K} \epsilon_1^\mu \epsilon_3^{*\nu} \frac{1}{u - m_K^2} (2p_4 - p_1)_\mu (2p_2 - p_3)_\nu, \end{aligned} \quad (5)$$

and

$$\begin{aligned} \mathcal{M}_{K^*}^{(g)} &= g_{\pi K^* K}^2 \epsilon_1^\mu \epsilon_2^\nu \frac{1}{t - m_K^2} (p_1 - 2p_3)_\mu (p_2 - 2p_4)_\nu, \\ \mathcal{M}_{K^*}^{(h)} &= g_{\pi K^* K}^2 \epsilon_1^\mu \epsilon_2^\nu \frac{1}{u - m_K^2} (p_1 - 2p_4)_\mu (p_2 - 2p_3)_\nu, \end{aligned} \quad (6)$$

respectively. Finally, the amplitudes for $K^*\bar{K}^* \rightarrow \rho\rho$ are

$$\begin{aligned} \mathcal{M}_{K^*}^{(i)} &= g_{\rho K^* K^*}^2 \epsilon_1^\alpha \epsilon_3^{*\beta} \epsilon_2^\gamma \epsilon_4^{*\delta} \frac{1}{t - m_{K^*}^2 + im_{K^*} \Gamma_{K^*}} \left(-g^{\mu\nu} + \frac{(p_1 - p_3)^\mu (p_1 - p_3)^\nu}{m_{K^*}^2} \right) \\ &\quad \times \left((2p_3 - p_1)_\alpha g_{\beta\mu} - (p_1 + p_3)_\mu g_{\alpha\beta} + (2p_1 - p_3)_\beta g_{\alpha\nu} \right) \left((p_2 + p_4)_\gamma g_{\delta\nu} + (p_2 - 2p_4)_\nu g_{\gamma\delta} + (p_4 - 2p_2)_\delta g_{\gamma\nu} \right), \\ \mathcal{M}_{K^*}^{(j)} &= g_{\rho K^* K^*}^2 \epsilon_1^\alpha \epsilon_4^{*\beta} \epsilon_2^\gamma \epsilon_3^{*\delta} \frac{1}{u - m_{K^*}^2 + im_{K^*} \Gamma_{K^*}} \left(-g^{\mu\nu} + \frac{(p_1 - p_4)^\mu (p_1 - p_4)^\nu}{m_{K^*}^2} \right) \\ &\quad \times \left((2p_4 - p_1)_\alpha g_{\beta\mu} - (p_1 + p_4)_\mu g_{\alpha\beta} + (2p_1 - p_4)_\beta g_{\alpha\nu} \right) \left((p_2 + p_3)_\gamma g_{\delta\nu} + (p_2 - 2p_3)_\nu g_{\gamma\delta} + (p_3 - 2p_2)_\delta g_{\gamma\nu} \right). \end{aligned} \quad (7)$$

In the above equations, p_i denotes the momentum of particle i . We keep the convention that particles 1 and 2 stand for initial-state mesons, and particles 3 and 4 final-state mesons on the left and right sides of the diagrams, respectively. The Mandelstam variables $s = (p_1 + p_2)^2$, $t = (p_1 - p_3)^2$, and $u = (p_1 - p_4)^2$ have also been used. We apply here the K^* meson propagator with its decay width, Γ_{K^*} , and use the isospin averaged value for the K^* meson decay width, $\Gamma_{K^*} = 49.1$ MeV [22].

In order to take the finite size of the hadron into consideration when evaluating amplitudes, we apply the following form factor at each interaction vertex for the u , t -channel and the s -channel, respectively,

$$F_{u,t}(\vec{q}) = \frac{\Lambda^2 - m_{ex}^2}{\Lambda^2 + \vec{q}^2}, \quad F_s(\vec{q}) = \frac{\Lambda^2 + m_{ex}^2}{\Lambda^2 + \omega^2}, \quad (8)$$

with \vec{q}^2 being the squared three-momentum transfer for t and u channels, and ω^2 being the total energy of the incoming particles for s channel taken in the center of mass frame. m_{ex} is the mass of the exchanged particle in each diagram shown in Fig. 1. We set the cutoff parameter Λ to be $\Lambda = 1.8$ GeV [23]. The final isospin- and spin-averaged cross section is given by,

$$\sigma = \frac{1}{64\pi^2 s g_1 g_2} \frac{|\vec{p}_f|}{|\vec{p}_i|} \int d\Omega |\overline{\mathcal{M}}|^2 F^4, \quad (9)$$

where g_1 and g_2 are the degeneracy factors of the initial 1 and 2 particles; $g_1 = (2I_1 + 1)(2S_1 + 1)$ and $g_2 = (2I_2 + 1)(2S_2 + 1)$, respectively. $|\overline{\mathcal{M}}|^2$ represents the squared amplitude of all processes in Eq. (2) obtained by summing over the isospins and spins of both the initial and final particles. $|\vec{p}_i|$ and $|\vec{p}_f|$ in Eq. (9) stand for the three-momenta of the initial and final particles in the center-of-mass frame.

Using the same method, we investigate hadronic effects on a K meson during the hadronic stage in heavy ion collisions. We consider interactions of the K meson with pions, ρ , K , and K^* mesons; $K\pi \rightarrow \rho K^*$, $K\rho \rightarrow \pi K^*$, $K\bar{K} \rightarrow \pi\pi$, $K\bar{K} \rightarrow \rho\rho$, and $K\bar{K}^* \rightarrow \pi\rho$. Among these, however, two processes $K\pi \rightarrow \rho K^*$, $K\rho \rightarrow \pi K^*$, are same as the inverse processes of the K^* meson interacting with ρ mesons and pions as shown in Fig. 1; (c) and (d), (a) and (b), respectively, and the process $K\bar{K}^* \rightarrow \pi\rho$ is same as that of the K^* meson interacting with \bar{K} mesons, diagrams (e) and (f) shown in Fig. 1. Therefore, all we need to consider more are the following amplitudes,

$$\begin{aligned} \mathcal{M}_{\bar{K}K \rightarrow \pi\pi} &\equiv \mathcal{M}_K^{(a)} + \mathcal{M}_K^{(b)}, \\ \mathcal{M}_{\bar{K}K \rightarrow \rho\rho} &\equiv \mathcal{M}_K^{(c)} + \mathcal{M}_K^{(d)}, \end{aligned} \quad (10)$$

for processes $K\bar{K} \rightarrow \pi\pi$ and $K\bar{K} \rightarrow \rho\rho$. We show the diagrams for these processes in Fig. 2.

The amplitudes for processes $K\bar{K} \rightarrow \pi\pi$ and $K\bar{K} \rightarrow \rho\rho$ are

$$\mathcal{M}_K^{(a)} = \frac{g_{\pi K^* K}^2}{t - m_{K^*}^2 + im_{K^*}\Gamma_{K^*}} (p_1 + p_3)_\mu (p_2 + p_4)_\nu$$

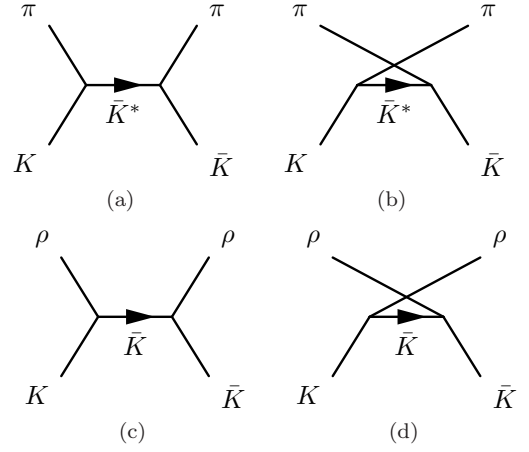


FIG. 2: Born diagrams for the K meson absorption by \bar{K} mesons: $K\bar{K} \rightarrow \pi\pi$, (a) and (b); $K\bar{K} \rightarrow \rho\rho$, (c) and (d).

$$\begin{aligned} &\times \left(-g^{\mu\nu} + \frac{(p_1 - p_3)^\mu (p_1 - p_3)^\nu}{m_{K^*}^2} \right), \\ \mathcal{M}_K^{(b)} &= \frac{g_{\pi K^* K}^2}{u - m_{K^*}^2 + im_{K^*}\Gamma_{K^*}} (p_1 + p_4)_\mu (p_2 + p_2)_\nu \\ &\times \left(-g^{\mu\nu} + \frac{(p_1 - p_4)^\mu (p_1 - p_4)^\nu}{m_{K^*}^2} \right), \end{aligned} \quad (11)$$

and

$$\begin{aligned} \mathcal{M}_K^{(c)} &= g_{\rho K K}^2 \epsilon_3^{*\mu} \epsilon_4^{*\nu} \frac{1}{t - m_K^2} (2p_1 - p_3)_\mu (2p_2 - p_4)_\nu, \\ \mathcal{M}_K^{(d)} &= g_{\rho K K}^2 \epsilon_4^{*\mu} \epsilon_3^{*\nu} \frac{1}{u - m_K^2} (2p_1 - p_4)_\mu (2p_2 - p_3)_\nu, \end{aligned} \quad (12)$$

respectively. Then, using Eqs. (8) and (9) we evaluate the K meson absorption cross sections.

Lastly we consider the possibility of the K^* meson formation from pions and kaons. The scattering cross section for the K^* meson production is given by the spin-averaged relativistic Breit-Wigner cross section;

$$\sigma_{K\pi \rightarrow K^*} = \frac{g_{K^*}^2}{g_K g_\pi} \frac{4\pi}{p_{cm}^2} \frac{s \Gamma_{K^* \rightarrow K\pi}^2}{(m_{K^*} - \sqrt{s})^2 + s \Gamma_{K^* \rightarrow K\pi}^2}, \quad (13)$$

with g_π , g_K , and g_{K^*} being the degeneracy of pions, K , and K^* mesons, $g_i = (2S_i + 1)(2I_i + 1)$, respectively, and p_{cm} the momentum in the center-of-mass frame. $\Gamma_{K^* \rightarrow K\pi}$ is the total decay width for a reaction $K\pi \rightarrow K^* \rightarrow K\pi$ as a function of \sqrt{s} . We take the following \sqrt{s} -dependent decay width $\Gamma_{K^* \rightarrow K\pi}$ of the K^* meson;

$$\Gamma_{K^* \rightarrow K\pi}(\sqrt{s}) = \frac{g_{\pi K^* K}^2}{2\pi s} p_{cm}^3(\sqrt{s}), \quad (14)$$

We show in Fig. 3 the cross sections for the absorption of both the K^* meson and the K meson by pions, ρ , K ,

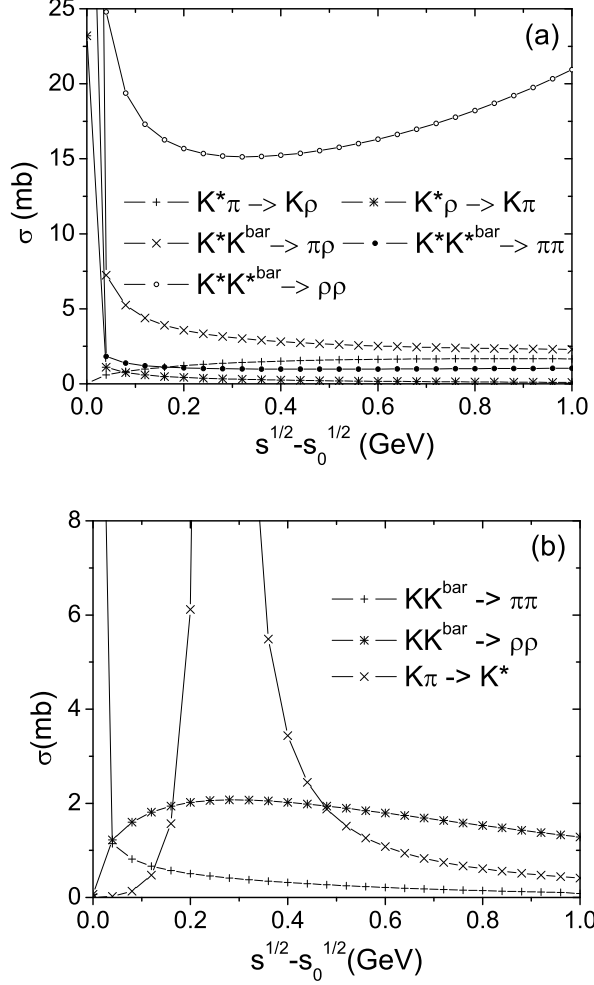


FIG. 3: Absorption cross sections for (a) the K^* meson by pions, ρ , K , and K^* mesons via processes $K^*\pi \rightarrow \rho K$, $K^*\rho \rightarrow \pi K$, $K^*\bar{K} \rightarrow \pi\pi$, $K^*\bar{K}^* \rightarrow \pi\pi$, and $K^*\bar{K}^* \rightarrow \rho\rho$, and those for (b) the K meson via processes $K\bar{K} \rightarrow \pi\pi$, $K\bar{K} \rightarrow \rho\rho$, and $K\pi \rightarrow K^*$.

and K^* mesons via processes shown in Fig. 1 and Fig. 2 as functions of the total center-of-mass energy $s^{1/2}$ above the threshold energy $s_0^{1/2}$ of each process. We see in Fig. 3 the general pattern that the cross sections have a peak near the threshold energy for the endothermic processes, e.g., $K^*\pi \rightarrow \rho K$ and $K\bar{K} \rightarrow \rho\rho$, while the cross sections for the exothermic processes, e.g., $K^*\rho \rightarrow \pi K$, $K^*\bar{K} \rightarrow \rho\pi$, $K^*\bar{K}^* \rightarrow \pi\pi$, $K^*\bar{K}^* \rightarrow \rho\rho$, and $K\bar{K} \rightarrow \pi\pi$, become infinite near the threshold. However, two endothermic

processes considered here, $K^*\pi \rightarrow \rho K$ and $K\bar{K} \rightarrow \rho\rho$ show very broad peaks above the threshold energy.

We notice that K^* meson is absorbed more by pions than by ρ mesons; the absorption cross section of the K^* meson by pions, $K^*\pi \rightarrow \rho K$ is larger than that by ρ mesons $K^*\rho \rightarrow \pi K$. We also see that the annihilation cross sections for both the K^* meson and K meson are larger when ρ mesons are produced than when pions are produced; the cross section for $K^*\bar{K}^* \rightarrow \rho\rho$ is larger than that for $K^*\bar{K}^* \rightarrow \pi\pi$, and the cross section for $K\bar{K} \rightarrow \rho\rho$ is also larger than that for $K\bar{K} \rightarrow \pi\pi$.

The cross section for $K^*\bar{K}^* \rightarrow \rho\rho$ is an order of magnitude larger than other processes, and seems to reflect the effect from two interaction mechanisms between three vector mesons. All particles participating in the process $K^*\bar{K}^* \rightarrow \rho\rho$ are vector mesons, and thus two $\mathcal{L}_{\rho K^* K^*}$ in Eq. (1) are needed to describe the process $K^*\bar{K}^* \rightarrow \rho\rho$. It has already been shown that the interaction between three vector mesons increases the absorption cross section in the effective Lagrangian approach [17].

It seems awkward to observe that the cross section for $K^*\bar{K}^* \rightarrow \rho\rho$ should rise with increasing energy even though the form factor has been correctly used to kill the artificial growth of the cross section with the energy. This behavior reminds the rise of the total cross section for $p\bar{p}$ collisions at high energy. It has been already well known that the resonance exchange is largely responsible for an increase of the cross section in high energy scattering. In this study the K^* meson exchange in the reaction $K^*\bar{K}^* \rightarrow \rho\rho$ causes the rise of cross section even at relatively low energy less than 1 GeV. The introduction of the decay width in the propagator Γ_{K^*} , however, does not contribute to this behavior at all. Instead it merely reduces a little bit the amplitudes for process having a K^* meson exchange. Finally, we also find that the cross section for the formation of the K^* meson from pions and K mesons, Eq. (13) is not small at all, compared to cross sections for other processes.

III. TIME EVOLUTIONS OF THE K^* AND K MESON ABUNDANCES

We consider the time evolutions of the abundance for both the K^* meson and kaon based on the cross sections evaluated in the previous section. We build a coupled evolution equation for both particles consisting of densities and abundances for mesons participating in all processes shown in Fig. 1; pions, ρ , K , and K^* mesons.

$$\begin{aligned} \frac{dN_{K^*}(\tau)}{d\tau} = & \langle \sigma_{K\rho \rightarrow K^*\pi} v_{K\rho} \rangle n_\rho(\tau) N_K(\tau) - \langle \sigma_{K^*\pi \rightarrow K\rho} v_{K^*\pi} \rangle n_\pi(\tau) N_{K^*}(\tau) \\ & + \langle \sigma_{K\pi \rightarrow K^*\rho} v_{K\pi} \rangle n_\pi(\tau) N_K(\tau) - \langle \sigma_{K^*\rho \rightarrow K\pi} v_{K^*\rho} \rangle n_\rho(\tau) N_{K^*}(\tau) \\ & + \langle \sigma_{\rho\pi \rightarrow K^*\bar{K}} v_{\rho\pi} \rangle n_\pi(\tau) N_\rho(\tau) - \langle \sigma_{K^*\bar{K} \rightarrow \rho\pi} v_{K^*\bar{K}} \rangle n_K(\tau) N_{K^*}(\tau) \end{aligned}$$

$$\begin{aligned}
& + \langle \sigma_{\pi\pi \rightarrow K^* \bar{K}^*} v_{\pi\pi} \rangle n_\pi(\tau) N_\pi(\tau) - \langle \sigma_{K^* \bar{K}^* \rightarrow \pi\pi} v_{K^* \bar{K}^*} \rangle n_{\bar{K}^*}(\tau) N_{K^*}(\tau) \\
& + \langle \sigma_{\rho\rho \rightarrow K^* \bar{K}^*} v_{\rho\rho} \rangle n_\rho(\tau) N_\rho(\tau) - \langle \sigma_{K^* \bar{K}^* \rightarrow \rho\rho} v_{K^* \bar{K}^*} \rangle n_{\bar{K}^*}(\tau) N_{K^*}(\tau) \\
& + \langle \sigma_{\pi K \rightarrow K^*} v_{\pi K} \rangle n_\pi(\tau) N_K(\tau) - \langle \Gamma_{K^*} \rangle N_{K^*}(\tau), \\
\frac{dN_K(\tau)}{d\tau} = & \langle \sigma_{\pi\pi \rightarrow K \bar{K}} v_{\pi\pi} \rangle n_\pi(\tau) N_\pi(\tau) - \langle \sigma_{K \bar{K} \rightarrow \pi\pi} v_{K \bar{K}} \rangle n_{\bar{K}}(\tau) N_K(\tau) \\
& + \langle \sigma_{\rho\rho \rightarrow K \bar{K}} v_{\rho\rho} \rangle n_\rho(\tau) N_\rho(\tau) - \langle \sigma_{K \bar{K} \rightarrow \rho\rho} v_{K \bar{K}} \rangle n_{\bar{K}}(\tau) N_K(\tau) \\
& + \langle \sigma_{K^* \pi \rightarrow K \rho} v_{K^* \pi} \rangle n_\pi(\tau) N_{K^*}(\tau) - \langle \sigma_{K \rho \rightarrow K^* \pi} v_{K \rho} \rangle n_\rho(\tau) N_K(\tau) \\
& + \langle \sigma_{K^* \rho \rightarrow K \pi} v_{K^* \rho} \rangle n_\rho(\tau) N_{K^*}(\tau) - \langle \sigma_{K \pi \rightarrow K^* \rho} v_{K \pi} \rangle n_\pi(\tau) N_K(\tau) \\
& + \langle \sigma_{\rho\pi \rightarrow K^* \bar{K}} v_{\rho\pi} \rangle n_\pi(\tau) N_\rho(\tau) - \langle \sigma_{K^* \bar{K} \rightarrow \rho\pi} v_{K^* \bar{K}} \rangle n_{\bar{K}}(\tau) N_{K^*}(\tau) \\
& + \langle \Gamma_{K^*} \rangle N_{K^*}(\tau) - \langle \sigma_{\pi K \rightarrow K^*} v_{\pi K} \rangle n_\pi(\tau) N_K(\tau), \tag{15}
\end{aligned}$$

where $n_i(\tau)$ is the density of a light meson i in the hadronic matter at proper time τ , and $N_j(\tau)$ is the abundance of the other light meson j in each process shown in Fig. 1 at proper time τ . $n_i(\tau)$ for pions and ρ mesons is evaluated from

$$\begin{aligned}
n_i(\tau) &= \frac{g_i}{2\pi^2} \int_0^\infty \frac{p^2 dp}{e^{\sqrt{p^2 + m_i^2}/T(\tau)} - 1} \\
&\approx \frac{g_i}{2\pi^2} m_i^2 T(\tau) K_2\left(\frac{m_i}{T(\tau)}\right), \tag{16}
\end{aligned}$$

by assuming that they are in thermal equilibrium, and varies in time through the temperature profile introduced below, Eq. (17). We obtain $N_j(\tau)$ by multiplying Eq. (16) by the hadronization volume $V(\tau)$. In Eq. (16), g_i is the degeneracy factor for a particle i and K_2 the modified Bessel function of the second kind.

$n_i(\tau)$ and $N_j(\tau)$ are functions of the proper time through the temperature profile developed to describe the dynamics of relativistic heavy ion collisions. We use the schematic model of a system with an accelerated transverse expansion based on the boost invariant Bjorken picture [19, 24].

$$\begin{aligned}
V(\tau) &= \pi[R_c + v_c(\tau - \tau_c) + a_c/2(\tau - \tau_c)^2]^2 \tau_c, \\
T(\tau) &= T_c - (T_h - T_f) \left(\frac{\tau - \tau_h}{\tau_f - \tau_h} \right)^{4/5}, \tag{17}
\end{aligned}$$

with T_h and τ_f being the hadronization temperature and the freeze-out time, respectively. Eq. (17) describes the system of the quark-gluon plasma expanding with its transverse velocity v_c and transverse acceleration a_c starting from its final transverse size R_c at the chemical freeze-out time τ_c . The temperature of the system decreases from the hadronization temperature to the kinetic freeze-out temperature T_f . The values used in Eq. (17) are summarized in Table I.

In the rate equations, Eq. (15), $\langle \sigma_{ab \rightarrow cd} v_{ab} \rangle$ is the thermally averaged cross section for initial two particles in a two-body process $ab \rightarrow cd$ given by [25]

$$\langle \sigma_{ab \rightarrow cd} v_{ab} \rangle$$

TABLE I: Values for the volume and temperature profiles in the schematic model Eq. (17).

Temp.(MeV)		Time (fm/c)
$R_c = 8.0$ fm	$T_c = 175$	$\tau_c = 5.0$
$v_c = 0.4c$	$T_h = 175$	$\tau_h = 7.5$
$a_c = 0.02c^2/\text{fm}$	$T_f = 125$	$\tau_f = 17.3$

$$\begin{aligned}
&= \frac{1}{1 + \delta_{ab}} \frac{\int d^3 \vec{p}_a d^3 \vec{p}_b f_a(\vec{p}_a) f_b(\vec{p}_b) \sigma_{ab \rightarrow cd} v_{ab}}{\int d^3 \vec{p}_a d^3 \vec{p}_b f_a(\vec{p}_a) f_b(\vec{p}_b)} \\
&= \frac{1}{1 + \delta_{ab}} \frac{T^4}{4m_a^2 K_2(m_a/T) m_b^2 K_2(m_b/T)} \\
&\times \int_{z_0}^\infty dz K_1(z) \sigma(z^2 T^2) \\
&\times [z^2 - (m_a + m_b)^2/T^2][z^2 - (m_a - m_b)^2/T^2], \tag{18}
\end{aligned}$$

with $z_0 = \max((m_a + m_b)/T, (m_c + m_d)/T)$, K_1 and K_2 being the modified Bessel function of the second kind, f_i being the Boltzmann momentum distribution of the particle i , $f_i(\vec{p}) = e^{-\sqrt{\vec{p}^2 + m_i^2}/T}$, respectively. v_{ab} is the relative velocity of interacting particles a and b , $v_{ab} = \sqrt{(p_a \cdot p_b)^2 - m_a^2 m_b^2}/(E_a E_b)$. $\langle \Gamma_{K^*} \rangle$ in Eq. (15) is the thermally averaged decay width of K^* mesons, Eq. (14), $\langle \Gamma_{K^*} \rangle = \Gamma_{K^*}(m_{K^*}) K_1(m_{K^*}/T)/K_2(m_{K^*}/T)$, which has been obtained in the same methods as used in Eq. (18).

The K^* meson abundance at τ , N_{K^*} , depends not only on the dissociation reactions like $K^* \pi \rightarrow \rho K$, $K^* \rho \rightarrow \pi K$, $K^* \bar{K} \rightarrow \rho \pi$, $K^* \bar{K}^* \rightarrow \pi \pi$, and $K^* \bar{K}^* \rightarrow \rho \rho$, but also on the production reactions, or the inverse reactions of the dissociation reactions, such as $\rho K \rightarrow K^* \pi$, $\pi K \rightarrow K^* \rho$, $\rho \pi \rightarrow K^* \bar{K}$, $\pi \pi \rightarrow K^* \bar{K}^*$, and $\rho \rho \rightarrow K^* \bar{K}^*$. We have taken both reactions into consideration in building the coupled equation for both the K^* meson and kaon in Eq. (15). We have used the detailed balance relation when evaluating thermally averaged cross sections of the inverse reactions from the results for forward processes shown in Fig. 3. The results are shown in Fig. 4.

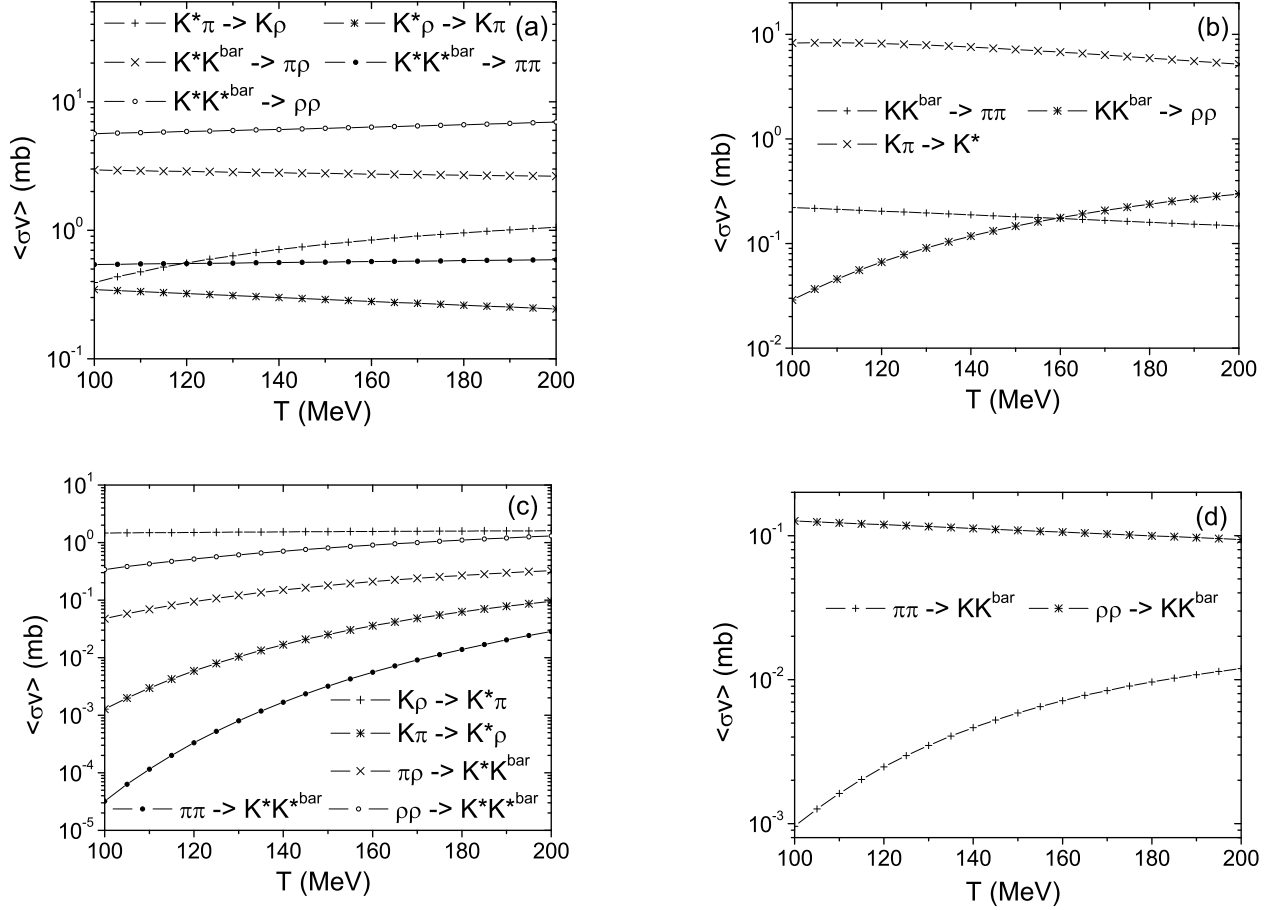


FIG. 4: Thermally averaged cross sections for the absorption of (a) a K^* meson by pions, ρ , K , and K^* mesons via processes $K^*\pi \rightarrow \rho K$, $K^*\rho \rightarrow \pi K$, $K^*\bar{K} \rightarrow \rho\pi$, $K^*\bar{K}^* \rightarrow \pi\pi$, and $K^*\bar{K}^* \rightarrow \rho\rho$, and those for (b) a K meson via processes $K\bar{K} \rightarrow \pi\pi$, $K\bar{K} \rightarrow \rho\rho$, and $K\pi \rightarrow K^*$. Thermally averaged cross sections for their inverse processes $\rho K \rightarrow K^*\pi$, $\pi K \rightarrow K^*\rho$, $\rho\pi \rightarrow K^*\bar{K}$, $\pi\pi \rightarrow K^*\bar{K}^*$, and $\rho\rho \rightarrow K^*\bar{K}^*$ for (c) a K^* meson, $\pi\pi \rightarrow K\bar{K}$ and $\rho\rho \rightarrow K\bar{K}$ for (d) a K meson.

As we see in Fig. 4, thermally averaged cross sections of the dissociation reactions are bigger than those of the production reactions for the exothermic reactions. In the case of the endothermic reaction like $K^*\pi \rightarrow \rho K$, thermalized production cross section is bigger than that for dissociation reaction. Both thermalized cross sections are comparable for the other endothermic reaction, $K\bar{K} \rightarrow \rho\rho$.

In general, the smaller threshold energy, mass, and degeneracy, the bigger thermally averaged cross section in the two-body process. We find that the thermally averaged cross section for K^* formation, $K\pi \rightarrow K^*$ becomes more significant than those for other reactions. However, the unusually rising cross section in energy for the reaction $K^*\bar{K}^* \rightarrow \rho\rho$ has been suppressed in the thermalized medium as shown in Fig. 4(a).

When solving the coupled differential equation for both the K^* meson and kaon abundances, we have treated

abundances of their antiparticles \bar{K}^* and \bar{K} mesons also as variables using the strangeness chemical potential μ_s ; i.e., $N_{\bar{K}^*} = e^{-2\mu_s/T(\tau)} N_{K^*}$ and same for antikaons. In other words, we have not considered that K^* mesons and kaons are in thermal equilibrium during the expansion of the hadronic matter, while we calculate the thermally averaged cross section Eq. (18) using the thermal distributions of hadrons involved. However, the initial yield of kaons at chemical freeze-out has been evaluated to be 88.1 using the statistical hadronization model, Eq. (16) with the strangeness chemical potential $\mu_s = 10$ MeV and the hadronization volume $V_H = 1908 \text{ fm}^3$ [20], whereas the initial yield of K^* mesons has been obtained from,

$$N_{K^*}(\tau) = V_H \frac{g_{K^*}}{2\pi^2} \int_{m_{th}}^{\infty} \frac{dm}{N_{BW}} \frac{\Gamma_{K^*}}{(m - m_{K^*})^2 + \Gamma_{K^*}^2/4} \times \int_0^{\infty} \frac{p^2 dp}{e^{(\sqrt{p^2 + m_{K^*}^2} - \mu_s)/T(\tau)} - 1}, \quad (19)$$

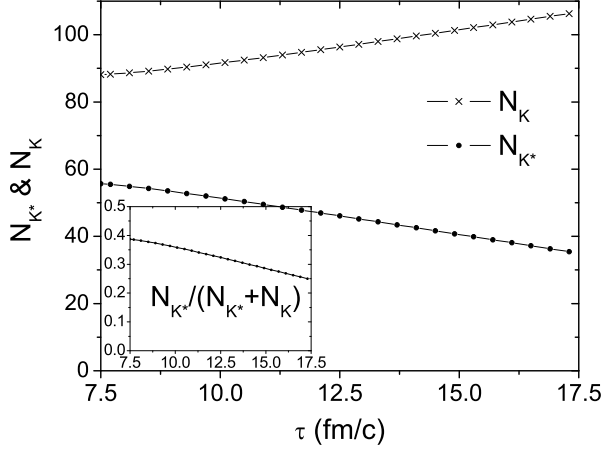


FIG. 5: Time evolution of the K^* meson and kaon abundances during the hadronic stage in central Au+Au collisions at $\sqrt{s_{NN}} = 200$ GeV. Ratio of the K^* meson abundance to the sum of the K^* meson and kaon abundances is shown in the inset.

to take the width of the K^* meson into consideration. In Eq. (19), m_{th} is the threshold energy for $K^* \rightarrow K\pi$ decay channel and N_{BW} is the normalization constant for the Breit-Wigner distribution. We obtain the K^* meson initial yield to be 55.7, which is slightly larger than 52.4 obtained without including the K^* meson width calculated with the formula given in Eq. (16).

In Fig. 5, we show the abundances of the K^* meson and kaon as a function of the proper time during the hadronic stage of heavy ion collisions at $\sqrt{s_{NN}} = 200$ GeV. As we have expected, the K^* meson abundance decreases due to both interactions of K^* mesons with other hadrons and the decay of the K^* meson to the pion and kaon, eventually becoming 35.6 at 9.8 fm/s after the chemical freeze-out. On the other hand the abundance of the kaon increases up to 106.5 at the end of hadronic expansion. We find that throughout the time evolution the sum of the K^* meson and kaon abundances changes slightly from 143.8 to 142.1. We also show in the inset of Fig. 5 the variation of the ratio of the K^* meson abundance to the sum of the K^* meson and kaon abundances. The ratio decreases from the initial ratio from the statistical hadronization model 0.39 to 0.25 in the end.

Based on the analysis we find that about 36% of K^* mesons produced at chemical freeze-out disappear during the hadronic stage in heavy ion collisions, making the invariant mass reconstruction of the total K^* meson difficult. We further find that the hadronic interactions shown in both Fig. 1 and Fig. 2 explain about 6% of the K^* meson loss, and the K^* meson decay is largely responsible for the K^* meson reduction in the hadronic medium. Our result is comparable to the 30% reduction of the previous statistical model prediction 0.33 ± 0.01

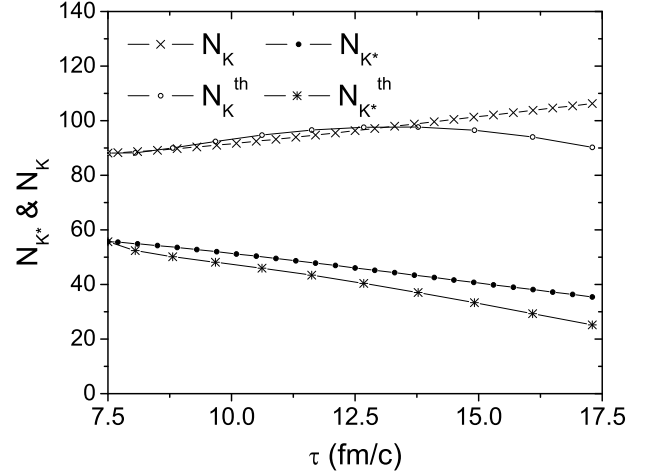


FIG. 6: A comparison between the K^* meson and kaon abundances due to all hadronic interactions shown in Fig. 1 and Fig. 2 and those from the thermal model prediction at each time and temperature.

[10] to the experimental measurements 0.23 ± 0.05 [13].

We also consider the possibility of both the K^* meson and kaon thermalization during the hadronic expansion. Assuming that both mesons are in thermal equilibrium with the hadronic medium we evaluate the K^* meson and kaon abundances in time using Eqs. (16), (19), and (17), and show the results represented by N_K^{th} and $N_{K^*}^{th}$ in Fig. 6.

As we see, $N_{K^*}^{th}$ keeps decreasing all the time. However, N_K^{th} increases at the beginning of the hadronic stage, and finally decreases. This is due to the competition between the volume expansion and the decreasing rate caused by the thermal effects in Eq. (16), through the factor $m_K/T(\tau)$ inside the modified Bessel function of the second kind, implying that N_K^{th} and $N_{K^*}^{th}$ depends on the size and also on the lifetime of the expanding fireball, Eq. (17). Nevertheless, one should note that the volume of the system expands in time with the total entropy almost preserved [26]. We find that abundances of most hadrons decrease during the hadronic expansion in the statistical hadronization model but that of the pion, the lightest hadron, increases in time to compensate the loss of entropy from heavier hadrons. We argue that the same mechanism is happening to strangeness hadrons for some time during the hadronic expansion. However, the ratio $N_{K^*}^{th}/(N_K^{th} + N_{K^*}^{th})$ is not affected by the volume, and it keeps decreasing from 0.39 to 0.22 at the kinetic freeze-out.

We notice that recent measurements of the K^* meson yield in Pb+Pb collisions at $\sqrt{s_{NN}} = 2.76$ TeV at the Large Hadron Collider (LHC) [27] provide 0.19 ± 0.05 as the K^{*0}/K^- ratio. This value is also smaller than the statistical hadronization model prediction 0.30 evaluated with the hadronization temperature 156 MeV [28] at the

LHC energy. The measurements indicate that more K^* mesons are lost during the hadronic expansion at LHC, leading to 37% reduction of the ratio.

IV. THE ABUNDANCE RATIO OF K^* MESONS TO KAONS IN HEAVY ION COLLISIONS

Since the interactions of K^* mesons and kaons with light mesons considered in Fig. 1 and Fig. 2 take place during the hadronic stage at both RHIC and LHC, it is necessary to understand general features of the variation of the K^* meson abundance in heavy ion collisions. In order to analyze the reduction of the K^* meson in the hadronic medium we simplify the coupled equation, Eq. (15) by keeping the linear terms in N_K and N_{K^*} only.

$$\begin{aligned}\frac{dN_{K^*}(\tau)}{d\tau} &= \gamma_K N_K(\tau) - \gamma_{K^*} N_{K^*}(\tau), \\ \frac{dN_K(\tau)}{d\tau} &= -\gamma_K N_K(\tau) + \gamma_{K^*} N_{K^*}(\tau),\end{aligned}\quad (20)$$

with

$$\begin{aligned}\gamma_{K^*} &= \langle \sigma_{K^*\rho \rightarrow K\pi} v_{K^*\rho} \rangle n_\rho + \langle \sigma_{K^*\pi \rightarrow K\rho} v_{K^*\pi} \rangle n_\pi \\ &\quad + \langle \Gamma_{K^*} \rangle, \\ \gamma_K &= \langle \sigma_{K\pi \rightarrow K^*\rho} v_{K\pi} \rangle n_\pi + \langle \sigma_{K\rho \rightarrow K^*\pi} v_{K\rho} \rangle n_\rho \\ &\quad + \langle \sigma_{K\pi \rightarrow K^*} v_{K\pi} \rangle n_\pi.\end{aligned}\quad (21)$$

When the thermal cross sections and densities of light mesons are independent of time, following analytic solutions are obtained from the coupled equation, Eq. (20),

$$\begin{aligned}N_{K^*}(\tau) &= \frac{\gamma_K}{\gamma} N^0 + \left(N_{K^*}^0 - \frac{\gamma_K}{\gamma} N^0 \right) e^{-\gamma(\tau-\tau_h)}, \\ N_K(\tau) &= \frac{\gamma_{K^*}}{\gamma} N^0 + \left(N_K^0 - \frac{\gamma_{K^*}}{\gamma} N^0 \right) e^{-\gamma(\tau-\tau_h)}\end{aligned}\quad (22)$$

where the initial yields for both hadrons, N_K^0 and $N_{K^*}^0$ have been assumed, and N^0 is the sum of the K^* meson and kaon yields, $N^0 = N_K^0 + N_{K^*}^0$ at chemical freeze-out. The γ in Eq. (22) is the sum of the K^* meson and kaon widths in the hadronic phase, $\gamma = \gamma_K + \gamma_{K^*}$; γ_{K^*} and γ_K play roles of the collisional broadening of the width of the K^* meson and kaon in the hadronic medium, respectively.

In Eq. (22) time-independent terms represent abundances when time goes to infinity, and the sum of two solutions is preserved as its initial value $N_K^0 + N_{K^*}^0$. As time goes on N_K increases while N_{K^*} decreases, and the rate at which the final number is reached in Eq. (22) is determined by the γ which takes into account hadronic interactions of K^* mesons and kaons with light mesons. If the γ is large, the abundance can change significantly for a short time.

Let us now investigate the time evolution of yield ratio of K^* mesons to kaons from the analytic solution of Eq.

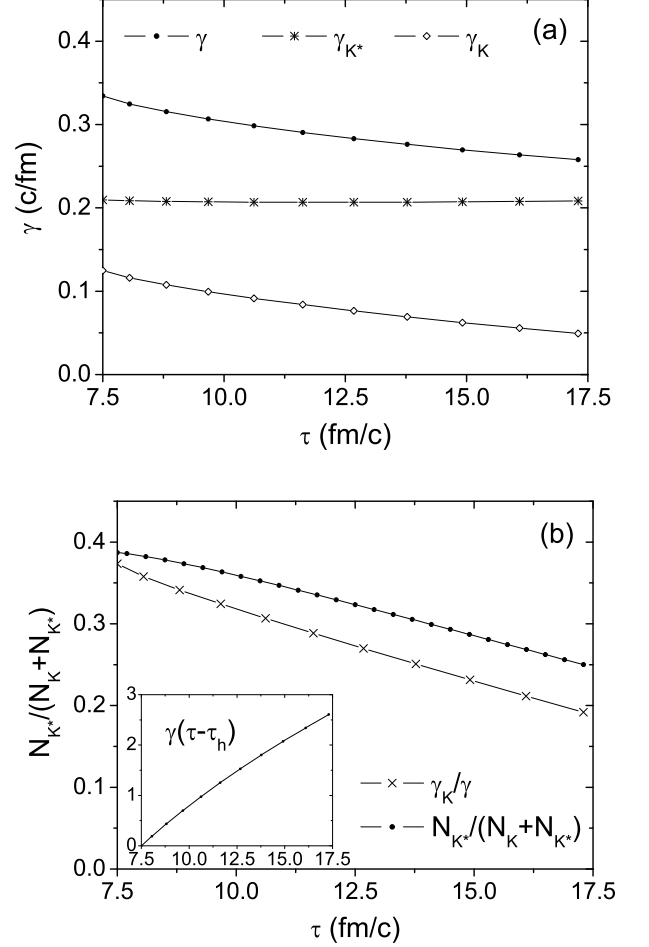


FIG. 7: (a) Variations of γ_K , γ_{K^*} , and $\gamma = \gamma_K + \gamma_{K^*}$ in time during the hadronic stage. (b) A comparison of the abundance ratio variation $N_{K^*}/(N_K + N_{K^*})$ obtained numerically from Eq. (15) for RHIC and $R(\tau = \infty) = \gamma_K/\gamma$ from Eq. (23) evaluated at each time and temperature. We show in the inset how $\gamma(\tau - \tau_h)$ changes in time.

(22), $R(\tau) = N_{K^*}(\tau)/(N_K(\tau) + N_{K^*}(\tau))$;

$$\begin{aligned}R(\tau) &= \frac{N_{K^*}(\tau)}{N_K(\tau) + N_{K^*}(\tau)} = \frac{N_{K^*}(\tau)}{N^0} \\ &= \frac{\gamma_K}{\gamma} + \left(\frac{N_{K^*}^0}{N^0} - \frac{\gamma_K}{\gamma} \right) e^{-\gamma(\tau-\tau_h)}.\end{aligned}\quad (23)$$

We notice that $R(\tau)$ is also composed of two parts; a time-independent part and a transient part. After a long time τ the time-independent part $R(\infty) = \gamma_K/\gamma$ is expected to represent the K^* meson to the kaon ratio. How fast the abundance ratio approaches the time-independent part relies on γ , the sum of the K^* meson and kaon widths in the exponential function.

With these in mind let us investigate the variation in the abundance of K^* mesons and kaons obtained from Eq. (15). Since all thermally averaged cross sections and

densities of the light mesons in γ_K and γ_{K^*} are functions of a time, solutions of Eq. (15) are different from the analytic solution of the simplified equation, Eq. (20). Nevertheless, we find that the solution of Eq. (15) keeps the same important characteristics of the analytic solutions from Eq. (20).

We first show in Fig. 7(a) γ 's obtained at Eq. (15) as a function of time. The γ decreases in time from 0.33 c/fm to 0.26 c/fm as the system cools down from 175 MeV at τ_H to 125 MeV at τ_f , reflecting that interactions between hadrons become less vigorous as the temperature of the system decreases. The γ_K , or $\langle\sigma_{K\pi\rightarrow K^*\rho}v_{K\pi}\rangle n_\pi + \langle\sigma_{K\rho\rightarrow K^*\pi}v_{K\rho}\rangle n_\rho + \langle\sigma_{K\pi\rightarrow K^*v_{K\pi}}\rangle n_\pi$ in Eq. (21) decreases as the temperature decreases, but γ_{K^*} is almost constant during the hadronic stage; with decreasing temperature of the system, the part of γ_{K^*} , or $\langle\sigma_{K^*\rho\rightarrow K\pi}v_{K^*\rho}\rangle n_\rho + \langle\sigma_{K^*\pi\rightarrow K\rho}v_{K^*\pi}\rangle n_\pi$ decreases whereas the thermal width of the K^* meson $\langle\Gamma_{K^*}\rangle$ slightly increases due to the factor $K_1(m_{K^*}/T)/K_2(m_{K^*}/T)$, meaning that K^* mesons live shorter at lower temperature.

We compare in Fig. 7(b) the abundance ratio variation $N_{K^*}/(N_K + N_{K^*})$ evaluated numerically from Eq. (15) for RHIC to γ_K/γ obtained from Eq. (23) at each time and temperature. γ_K/γ represents the expected hadronic interaction width ratio between kaons and K^* mesons plus kaons at each temperature and time. We anticipate that the abundance ratio of K^* mesons and kaons in Fig. 7 approaches to γ_K/γ as time goes on, like the ratio between those mesons obtained from the simplified rate equation, Eq. (23). We show in the inset of Fig. 7(b) how $\gamma(\tau - \tau_h)$ varies in time at RHIC. As we see, $\gamma(\tau - \tau_h)$ increases up to 2.5 for 9.8 fm/c. We expect that the similar term with $e^{-\gamma(\tau - \tau_h)}$ in the real solution suppresses the contribution of the time-dependent term as time goes on. The discrepancy between the abundance ratio and the γ_K/γ in Fig. 7(b) is attributable to both the contribution from non-linear terms included in Eq. (15) such as $K^*\bar{K} \rightarrow \rho\pi$, (e) and (f); $K^*\bar{K}^* \rightarrow \pi\pi$, (g) and (h); $K^*\bar{K}^* \rightarrow \rho\rho$, (i) and (j) shown in Fig. 1 and $K\bar{K} \rightarrow \pi\pi$, (a) and (b); $K\bar{K} \rightarrow \rho\rho$, (c) and (d) shown in Fig. 2, and the time delay required to reach thermal equilibrium from the interactions of K^* mesons with light mesons in the hadronic medium.

Based on the above analysis we argue that the final ratio of the yield between K^* mesons and kaons in heavy ion collisions is largely dependent on their interactions with other hadrons in the hadronic medium, γ_K and γ_{K^*} . Since $\gamma(\tau - \tau_h)$ keeps increasing during the hadronic stage, the transient term with $e^{-\gamma(\tau - \tau_h)}$ in the yield ratio $R(\tau)$ plays a negligible role at a later time during the hadronic interaction stage. Therefore, we see that the relative interaction ratio γ_K/γ mainly determines the final yield ratio between K^* mesons and kaons at the end of the hadronic stage.

We show in Fig. 8 γ_K/γ as a function of the temperature of the system. We also show in Fig. 8 measurements of the abundance ratio between K^* mesons and

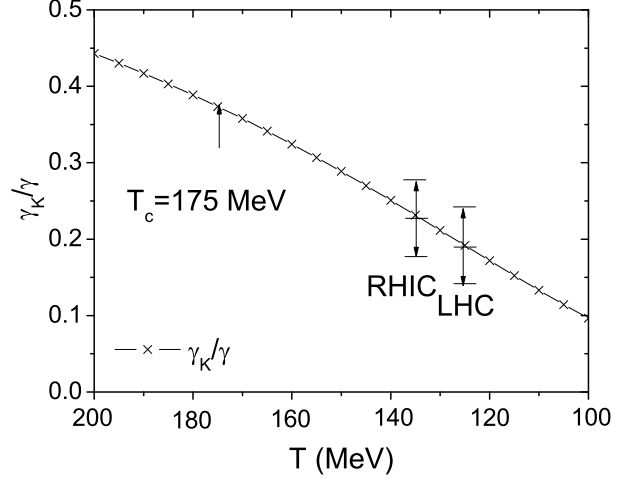


FIG. 8: A variation of the γ_K/γ in temperature during the hadronic stage. We show measurements of the abundance ratio between K^* mesons and kaons, $N_{K^*}/(N_K + N_{K^*})$ 0.23 ± 0.05 at RHIC [13] and 0.19 ± 0.05 at LHC [27]

kaons, $N_{K^*}/(N_K + N_{K^*})$, 0.23 ± 0.05 at RHIC [13] and 0.19 ± 0.05 at LHC [27]. We notice from Fig. 8 that the ratio of the K^* meson and kaon in heavy ion collisions seems to reflect the interaction ratio between strange and light mesons, γ_K/γ at the kinetic freeze-out temperature. We infer that the lower ratio $N_{K^*}/(N_K + N_{K^*})$ at LHC compared to that at RHIC is due to a lower kinetic freeze-out temperature at LHC than at RHIC.

It has been argued that the degree of the reduction of K^* meson yield during the hadronic stage in heavy ion collisions is attributable to a lifetime of the hadronic stage. Since the system of quark-gluon plasma at LHC is much larger than that at RHIC, it has been assumed that the lifespan of the hadronic stage at LHC is also longer compared to that at RHIC, and thereby more K^* meson are lost in the hadronic medium at LHC.

We find, however, from the investigation of the variation in the yield ratio between K^* mesons and kaons based on the solution of the rate equation, that the reduction of the K^* meson in heavy ion collisions reflects the interaction of K^* mesons and kaons with light mesons at kinetic freeze-out. We argue that the degree of the K^* meson abundance reduction in heavy ion collisions, or the reduction of the yield ratio between the K^* meson and kaon, is largely attributable to the *kinetic freeze-out temperature* via the interaction of K^* mesons and kaons with light mesons in the hadronic medium. The long lifespan of the hadronic stage just suppresses more a transient term, such as the second term in Eq. (23), contributing little to the change of the K^* meson to kaon ratio.

As has been already mentioned, how fast meson abundances change in the hadronic medium is governed by the sum of all the interactions involved, i.e., the width γ in Eq. (22). Therefore, in addition to the hadronic inter-

actions considered in Figs. 1 and 2 all other interactions with various hadrons, i.e., nucleons, have to be taken into account to thoroughly understand the reduction of K^* mesons in heavy ion collisions. Moreover, we also have to include more the feed down effects from heavier strangeness hadrons to fully consider the abundance ratio of the K^* meson to the kaon, which are left for the future work.

V. CONCLUSION

We have studied the reduction of K^* mesons in heavy ion collisions. We have focused on the hadronic effects on the K^* meson and kaon abundances during the hadronic stage of the central Au+Au collisions at $\sqrt{s_{NN}} = 200$ GeV in order to understand the K^* meson yield difference between the experimental measurement and the statistical hadronization model prediction. We have evaluated absorption cross sections for both kaons and K^* mesons by pions, ρ , K , and K^* mesons inside the hadronic medium. In describing the interaction between K^* mesons and kaons and light mesons, we have introduced one meson exchange model with the effective Lagrangian. Furthermore, we have built the coupled differential equation for K^* mesons and kaons, and have solved it to investigate the time evolution of the K^* meson and kaon abundances during the expansion of the hadronic matter.

We have found that the K^* meson and kaon abundances during the hadronic stage of heavy ion collisions are dependent on absorption cross sections and their thermal average. We have shown that the sum of K^* and kaon abundances are almost preserved during the expansion, and the interaction of K^* mesons with light mesons controls the reduction or production of K^* mesons and kaons in the hadronic matter. Our analysis indicates that 36% of the total K^* mesons produced at the chemical freeze-out are lost during the hadronic expansion in the

central Au+Au collisions at $\sqrt{s_{NN}} = 200$ GeV. We have found that among 36% about 6% of the total K^* mesons are converted into light mesons by hadronic interactions, and the remaining 30% reduction is due to the decay of K^* mesons to kaons and pions. We see that the loss of the K^* meson abundance in the hadronic medium explains very well the discrepancy of the K/K^* ratio between the statistical hadronization [10] model prediction and the experimental measurements [13].

We have shown that the results obtained here can be applied to the analysis of the K^* meson production at the LHC. We have found that all the interactions involved at RHIC must be present at LHC, and therefore widths γ_{K^*} and γ_K evaluated at the RHIC energy can be applied to the case at the LHC energy. Moreover, we have realized that the smaller ratio of K^*/K measured at the LHC energy indicates a lower temperature of the kinetic freeze-out at LHC compared to that at RHIC. We have shown that the yield ratio between K^* mesons and kaons is not mainly dependent on the lifetime of the hadronic stage in heavy ion collisions, and the hadronic interaction width ratio of strange mesons with light mesons, γ_K/γ determines the final yield ratio between K^* mesons and kaons. We therefore conclude that studying the yield of the K^* meson and its variation during the hadronic stage in relativistic heavy ion collisions provides a chance to understand not only the production of K^* mesons but also the evolution of the hadronic medium in heavy ion collisions.

Acknowledgements

S. Cho was supported by 2015 Research Grant from Kangwon National University. S. H. Lee was supported by the Korea National Research Foundation under the grant number KRF-2011-0020333 and KRF-2011-0030621.

-
- [1] I. Arsene *et al.* (BRAHMS Collaboration), Nucl. Phys. A **757**, 1 (2005).
 - [2] B. B. Back *et al.* (PHOBOS Collaboration), Nucl. Phys. A **757**, 28 (2005).
 - [3] J. Adams *et al.* (STAR Collaboration), Nucl. Phys. A **757**, 102 (2005).
 - [4] K. Adcox *et al.* (PHENIX Collaboration), Nucl. Phys. A **757**, 184 (2005).
 - [5] M. Gyulassy and L. McLerran, Nucl. Phys. A **750**, 30 (2005).
 - [6] S. Gupta, X. Luo, B. Mohanty, H. G. Ritter, and N. Xu, Science, **332**, 1525 (2011).
 - [7] P. Braun-Munzinger, J. Stachel, J. P. Wessels, and N. Xu, Phys. Lett. B **344**, 43 (1995).
 - [8] P. Braun-Munzinger, J. Stachel, J. P. Wessels, and N. Xu, Phys. Lett. B **365**, 1 (1996).
 - [9] P. Braun-Munzinger, I. Heppe, and J. Stachel, Phys. Lett. B **465**, 15 (1999).
 - [10] P. Braun-Munzinger, D. Magestro, K. Redlich, and J. Stachel, Phys. Lett. B **518**, 41 (2001).
 - [11] G. Torrieri and J. Rafelski, Phys. Lett. B **509**, 239 (2001).
 - [12] M. Bleicher and J. Aichelin, Phys. Lett. B **530**, 81 (2002).
 - [13] J. Adams *et al.* (STAR Collaboration), Phys. Rev. C **71**, 064902 (2005).
 - [14] M. M. Aggarwal *et al.* (STAR Collaboration), Phys. Rev. C **84**, 034909 (2011).
 - [15] S. G. Matinyan and B. Muller, Phys. Rev. C **58**, 2994 (1998).
 - [16] K. L. Haglin, Phys. Rev. C **61**, 031902(R) (2000).
 - [17] Z. Lin and C. M. Ko, Phys. Rev. C **62**, 034903 (2000).
 - [18] Y. Oh, T. Song, and S. H. Lee, Phys. Rev. C **63**, 034901 (2001).
 - [19] L. W. Chen, C. M. Ko, W. Liu, and M. Nielsen, Phys. Rev. C **76**, 014906 (2007).
 - [20] S. Cho and S. H. Lee, Phys. Rev. C **88**, 054901 (2013).
 - [21] A. M. Torres, K. P. Khemchandani, F. S. Navarra, M.

- Nielsen and L. M. Abreu, Phys. Rev. D **90**, 11, 114023 (2014)
- [22] J. Beringer *et al.* (Particle Data Group Collaboration), Phys. Rev. D **86**, 010001 (2012)
- [23] G. E. Brown, C. M. Ko, Z. G. Wu and L. H. Xia, Phys. Rev. C **43**, 1881 (1991).
- [24] L-W. Chen, V. Greco, C. M. Ko, S. H. Lee, and W. Liu, Phys. Lett. B **601**, 34 (2004)
- [25] P. Koch, B. Muller and J. Rafelski, Phys. Rept. **142**, 167 (1986).
- [26] P. J. Siemens and J. I. Kapusta, Phys. Rev. Lett. **43**, 1486 (1979).
- [27] B. B. Abelev *et al.* (ALICE Collaboration), Phys. Rev. C **91**, 2, 024609 (2015).
- [28] J. Stachel, A. Andronic, P. Braun-Munzinger and K. Redlich, J. Phys. Conf. Ser. **509**, 012019 (2014).